



Optimization of Electrode Material Composition from Activated Carbon, MWCNT & Graphene to Enhance Performance of Supercapacitor

Heri Rustamaji^{1,2}, Tirto Prakoso^{1*}, Hary Devianto¹, Pramujo Widiatmoko¹ & Isdiriyani Nurdin¹

¹Department of Chemical Engineering, Faculty of Industrial Technology
Institut Teknologi Bandung, Jalan Ganesa No.10, Bandung 40132, Indonesia

²Department of Chemical Engineering, Faculty of Engineering, Lampung University,
Jalan Soemantri Brojonegoro No.1, Bandar Lampung 35141, Indonesia

*E-mail: tirto@che.itb.ac.id

Highlights:

- A carbon nanocomposite was produced from activated carbon, MWCT, and graphene.
- Composite-based electrodes improve electric conductivity, reduce cell resistance and increase specific capacitance significantly.
- The composite material showed outstanding capacitance performance and maintained cell cycle stability.
- Composite materials strengthen the energy and power density of the supercapacitor.

Abstract. The supercapacitor has gotten a lot of attention as a high-performance energy storage device because of its high power density, good energy density, long life cycle, and extensive application in various electronic applications. To effectively assess its performance, the electrode material composition was optimized with a blend of activated carbon (AC), multiwall carbon nanotube (MWCNT), and graphene (GR). The synergistic effect of AC, CNT, and GR supports the usage of AC/MWCNT/GR as a viable supercapacitor electrode. Furthermore, the surrounding MWCNT enhances AC and GR electronic conductivity, while AC efficiently suppresses GR re-stacking sheets and aggregates MWCNT particles. For supercapacitor electrodes, the optimal composite mixtures of AC, MWCNT, and GR were 71.7%, 20%, and 8.3% wt, respectively. Meanwhile, an outstanding capacitance value of 33.5 F g⁻¹ in 6 M KOH electrolyte was obtained at 2 mV s⁻¹.

Keywords: *composite material; electrochemical performance; energy storage; nanocarbon; supercapacitor.*

1 Introduction

The supercapacitor has received massive attention as highly promising energy storage and conversion device due to its tremendous power density, fast storage

capability, prolonged life cycle, and effective use in numerous electronic applications, portable electronic devices, vehicles (both hybrid and electric), and large-scale industrial equipment [1-4].

Supercapacitors store energy depending on the electrostatic charge that accumulates at the electrochemical double-layer capacitor, such as carbon. The energy storage mechanism is also due to the reversible redox reactions of transition metal oxides and reversible doping/de-doping in conducting polymers or hybrid capacitors [5]. Therefore, the gravimetric surface area of the electrode, electrode conductivity, distribution of pore sizes, the electrolyte's electrochemical stability in the electrode, the resistance to the redox reaction on the surface of the electrode, operating voltage, electrolyte's resistance to electrodes, and electrolyte's grounding needs to be taken into account when deciding the electrode material for the supercapacitor [6].

Some of the various electrodes that have received significant attention are activated carbon, carbon nanotubes, and graphene materials [7-8]. About 80% of supercapacitors utilize nanocarbon as an electrode material [9]. Activated carbon material has the largest surface area with weak electrical conductivity and complex pores, leading to long-period ion diffusion pathways. Carbon nanotubes have a nano-sized tube structure and a mesoporous matrix that accelerates ion diffusion to the active surface of the composite [10-13]. Graphene is a two-dimensional material comprising carbon atoms organized in a honeycomb lattice. Its unique structure provides a massive theoretical specific surface area ($2675 \text{ m}^2\text{g}^{-1}$) with excellent thermal, mechanical and optical properties [14-16]. Some advantages of graphene include short diffusion distances due to its thinness (several angstroms), high surface-to-volume ratio, structural flexibility, open-pore systems, thermal and chemical stability, and compatibility with electrolytes over a significant electrochemical range [17]. Furthermore, this supercapacitor shows severe aggregation and re-stacking, decreasing effective surface area. The re-stacking process occurs because the ability of the van der Waals to interact with the adjacent sheets decreases the surface area and energy density [18].

In the literature review, no articles were found that discuss the composite material of activated carbon, CNT, and graphene. In this study, a supercapacitor performance test was carried out with electrode material from commercial activated carbon, multiwall carbon nanotube, graphene, and optimization of the electrode material mixture from the three materials to increase the supercapacitor performance.

Optimization of Electrode Material Composition from Activated Carbon, MWCNT & Graphene to Enhance Performance of Supercapacitor

2 Materials and Methods

2.1 Materials

The composite electrode material used in this study was primarily prepared from activated carbon (AC), multiwall carbon nanotube (MWCNT), and multilayer graphene (GR). Commercial AC was obtained from CV with the EstraChemical (Tangerang, Indonesia) consisting of a nominal BET (Brunauer, Emmett, and Teller) specific surface area, pore-volume, and average pore diameter are $832.9 \text{ m}^2 \text{ g}^{-1}$, $0.53 \text{ cm}^3 \text{ g}^{-1}$, and 4.05 nm , respectively. The MWCNT used are industrial grade with an outer and inner diameter, tube length, specific surface area, apparent density, and conductivity of 50 nm , $5\text{-}15 \text{ nm}$, $10\text{-}20 \text{ }\mu\text{m}$, $60 \text{ m}^2 \text{ g}^{-1}$, 0.19 g cm^{-3} , and 100 S m^{-1} , respectively from XFNano (Jiangsu, China). Industrial grade graphene nanoparticles are used with a specific surface area, apparent density, and conductivity of $31.657 \text{ m}^2 \text{ g}^{-1}$, $0.09\text{-}0.10 \text{ g cm}^{-3}$, and $550\text{-}1000 \text{ Sm}^{-1}$.

Potassium hydroxide (KOH, Merck, 99%), ethanol ($\text{C}_2\text{H}_5\text{OH}$, AR, 96%), polyvinylidene fluoride (PVDF, 65%), and Whatman filter paper were purchased from PT. Bratachem, Bandung. Xiamen TOB New Energy, China, provided the coin cell (CR2032) case and hydraulic crimping equipment.

2.2 Physical Characterization

The analysis of activated carbon, MWCNT, and graphene was characterized by scanning electron microscopy (SEM) using the SEM Hitachi SU3500. Furthermore, a Bruker D8 Advance powder diffractometer was used to determine the x-ray powder diffraction (XRD) using a 0.020 and $\text{Cu K}\alpha$ radiation step at 40 kV and 40 mA . SEM and XRD analysis was conducted in Research Center for Nanosciences and Nanotechnology, Bandung Institute of Technology (ITB). A Raman spectrophotometer with a blue laser beam of 532 nm (XploRa Plus) was used to produce the Raman spectra conducted at the Laboratory of Center for Mineral, Coal, and Geothermal Resources, ESDM-Bandung.

2.3 Coin-Cell Assembly and Electrochemical Characterization

The composite electrode material comprised AC, MWCNT, and GR with a composition variation and ten wt% PVDF (polyvinylidene fluoride) of mixture material. The particles were disseminated in ethanol and blended for half an hour using sonication. Furthermore, a circular electrode with a radius and thickness of 7.5 mm and 1 mm was formed by molding and pressing 0.2 g of the dry composite material at $7\text{-}10 \text{ Mpa}$. A supercapacitor of the type coin cell (CR2302) was arranged with symmetric electrodes at a composite material loading of 2.30 mg cm^{-2} . The two electrodes were separated in 6 M KOH using Whatman filter paper, and the cell was then squeezed using a hydraulic crimping machine.

A potentiostat (Gamry V3000) was used to determine the electrochemical behavior of samples. Electrochemical characterization consists of galvanostatic charge-discharge (GCD), cyclic voltammetry (CV), and electrochemical impedance spectroscopy (EIS) using a complete cell system. Meanwhile, the stability test was carried out by analyzing the cyclic charge-discharge of 5000 cycles at an applied current of 50 mA. The cell capacitance is determined using equation (1) from the CV curve [19].

$$C_{sp} = \frac{1}{mv|V_2-V_1|} \int_{t=0(V_1)}^{t(V_2)} i(V)dt \quad (1)$$

Where C_{sp} denotes the cell capacitance ($F g^{-1}$), V_2-V_1 is the voltage sweep (V), m is the total mass of active electrodes (g), v denotes the scan rate ($mV s^{-1}$), and $i(V)dt$ represents the area covered by the CV curve.

$$E = \frac{1}{2} \frac{C_{sp}}{3.6} V^2 \quad (2)$$

$$P = \frac{E \times 3600}{t_{disch}} \quad (3)$$

Meanwhile, energy density, E ($Wh kg^{-1}$), and power density, P ($W kg^{-1}$), were estimated from Eqs. (2) and (3), respectively, where V is the maximum voltage (V), and t_{disch} means discharge time (s).

3 Results and Discussion

3.1 Morphological and Structural Characterization

The morphologies of the individual and composite samples were characterized by scanning electron microscopy (SEM), as shown in Figure 1. SEM micrographs of the pure AC (Figure 1(a)) show a rock-like, less porous structure and exhibit the non-uniform structure of the agglomerated particle. It also corresponds to the moderate surface area of $832.9 m^2 g^{-1}$ with SEM micrographs of the pure MWCNT fiber (Figure 1(b)), presenting cylindrical and smooth cross-sections with neat MWCNT bundles. SEM micrographs of the pristine graphene shown in Figure 1(c) indicate that the graphene nanosheets became semi-transparent and consisted of multilayers. The nanosheet layers had sharp corners with well-defined edges.

Figure 1(d) shows a composite material comprised of AC, MWCT, and GR with a relatively even distribution of each material. Because of CNT's well-defined flexibility, the resulting AC/MWCNT/GR ternary nanocomposite system (S721) displayed homogeneity, and CNT was tightly wrapped around AC particles (Figure 1(d)). MWCNT also appeared to minimize GR particle re-stacking and

Optimization of Electrode Material Composition from Activated Carbon, MWCNT & Graphene to Enhance Performance of Supercapacitor

uniformly disseminate them. Thus, CNT was used to connect GR particles with CNT-wrapped AC particles, forming a consistent electrical conduction network of the ternary system [20].

X-ray diffraction (XRD) was utilized to arrange the structure of commercial samples. Figure 2(a) shows the XRD curves of three the materials, which reveal a most significant intensity peak at approximately $2\theta = 26.68^\circ$, 26.89° , and 26.53° for AC, WCNT, and GR, respectively. The values of MWCNT and GR indicate that these samples have a typical hexagonal graphitic structure. Meanwhile, AC with peaks at $2\theta = 26.68^\circ$ and 39.5° demonstrates that the example has a graphitized amorphous structure [21]. The 2θ peaks around 21° , 30° , 36° , 37° , and 39° in the XRD AC pattern are an indication of impurities in the form of minerals (such as Ca, Mg, Al, Fe, Si, K, Na, and Cl), which can come from the ash content of activated carbon precursor. This ash content cannot be lost entirely in the carbonization and activation process [22]. The presence of ash in the activated carbon synthesis process can reduce the specific surface area (porosity) but increase the degree of graphitization and electrical conductivity [23].

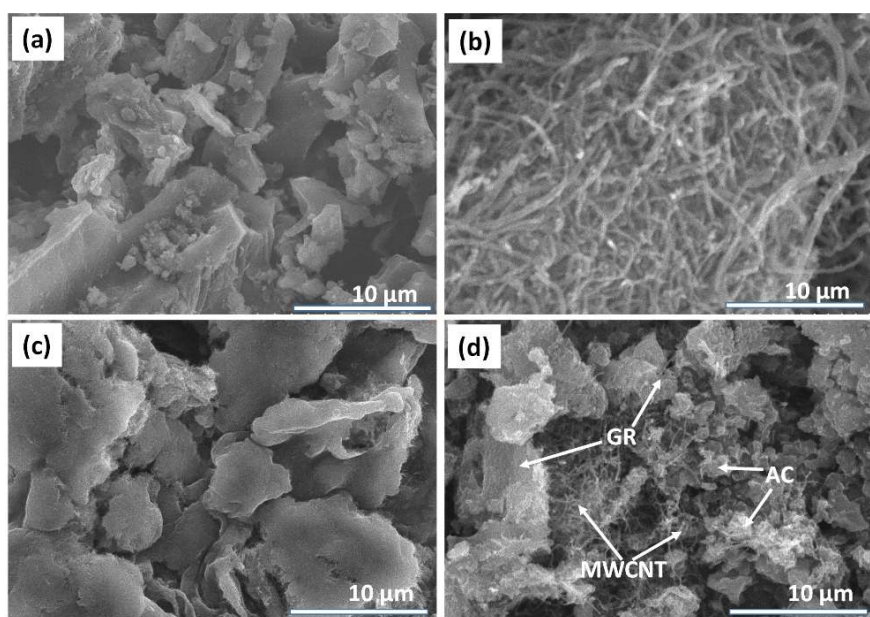


Figure 1 SEM image of (a) AC, (b) MWCNT, (c) GR, and (d) composite material.

Figure 2(b) demonstrates the Raman shift of pure carbon and composite material. For carbon material, two substantial peaks were discovered, centered at roughly

1592 cm^{-1} for graphitic (G) and 1342 cm^{-1} for the disordered (D) band, indicating that an idealized and uneven graphite lattice shows the Raman shift. The disruption band, also known as the D band, is formed by the sp^3 hybridized carbon at the graphene's edge and illustrates the severity of the graphite structural defect. The G band represented the sp^2 hybridized carbons coming from the C-C bond strain on the graphitic plane. The quantity of structural defects in heteroatoms associated with sp^3 carbon is explained by the D and G band ratios [24].

Bands of G, D, and 2D characterize graphene spectrums and MWCNT. Furthermore, the intensity ratios I_D/I_G and I_{2D}/I_G provide information about the structural disorder and graphene quality, where the defect-free graphene I_{2D}/I_G is equivalent to 2. Single-layer graphene could be verified using the single and sharp second-order Raman band (2D) at about 2700 cm^{-1} , frequently employed. Due to the breaking of the multilayer material's electrical band structure, the 2D band of multilayer graphene can be matched with many peaks. [25]. Graphene and MWCNT spectra in Figure 2(b) show 2D broad peaks, indicating multilayer graphene and multiwall CNT. Meanwhile, similar intensities of these D and G bands indicate a high quantity of structural defects. WMCNT had the lowest I_D/I_G ratio, followed by graphene, composites, and activated carbon. The composite material had a lower I_D/I_G value than activated carbon, indicating a lower degree of disorder or higher graphitization which could be due to the contribution of MWCT and GR.

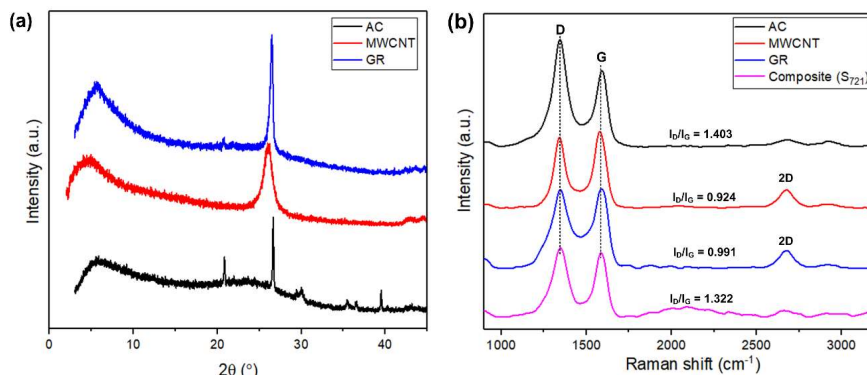


Figure 2 (a) XRD image of carbon material and (b) Raman spectra of carbon and composite material.

3.2 Electrochemical Performance

The electrochemical performance of each sample was evaluated using pure material in the complete cell system. Figure 3(a) illustrates the cyclic voltammograms (CV) and EDLC of varying electrodes at a 2 mV s^{-1} in a 6 M

Optimization of Electrode Material Composition from Activated Carbon, MWCNT & Graphene to Enhance Performance of Supercapacitor

KOH aqueous solution. It further shows that the CV of MWCNT and GR possess similar rectangular shapes and exhibit good symmetry, thereby indicating ideal capacitive behavior. The rectangular shape of CV also indicated that the primary electric and double layer capacitance (EDLC) are formed because of the numerous electrolyte ions adsorbed on the material's surface with limited electrolyte diffusion [26]. Meanwhile, CV curves for activated carbon (AC) show a slanted parallelogram shape, indicating rapid charge and discharge processes with low series resistance with high power capabilities [27]. The AC has the largest specific capacitance out of the three samples because of the linear relations between CV and capacitance. The supercapacitor with electrode material from AC, MWCNT, and GR by CV is 13.12 F g^{-1} , 3.93 F g^{-1} , and 7.86 F g^{-1} , respectively, as shown in Eq. (1).

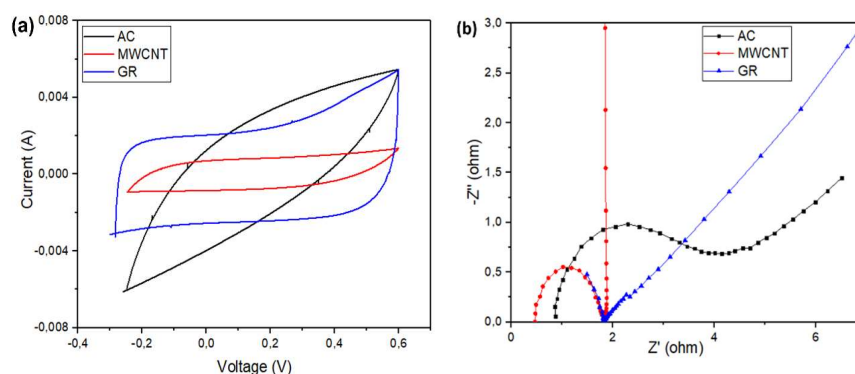


Figure 3 (a) CV curves of different samples at 2 mV s^{-1} in 6.0 M KOH aqueous electrolytes and (b) EIS Curve of the other samples with the entire Nyquist plot.

Figure 3(b) shows the Nyquist plots of EIS data used to test the EDLCs with different electrode types in KOH electrolytes. The imaginary component in the complex plane comprises the capacitive and ohmic properties denoted by $-Z''$ and Z' , respectively. A frequency of 100 kHz was used to study both features, with the plots consisting of more than one semicircle in the complex plane. The center of the semicircle is sometimes located under the Z' axis, while the type Nyquist plot of a supercapacitor comprises three regions concerning the frequencies. Furthermore, the supercapacitor has a character like a resistor at a very high frequency [28]. Contact resistance is observed between the electrode materials and the current collector (CR2032 case). Figure 4 shows that the center of the semicircle diameter is located between the first and second intercept points of the Z' axis along the Nyquist curve. Semicircle regions for AC, MWCNT, and GR electrodes had a resistance of 3, 1.4, and 1.5 ohms, respectively. The small matter located in the semicircle region indicates a low charge transfer resistance between

the electrolyte and the electrode and has good electrical transfer in the current collector. Figure 4 shows that supercapacitors with 100% activated carbon electrode material had the largest semicircle region. It has the lowest conductivity compared with MWCNT and GR upon activation.

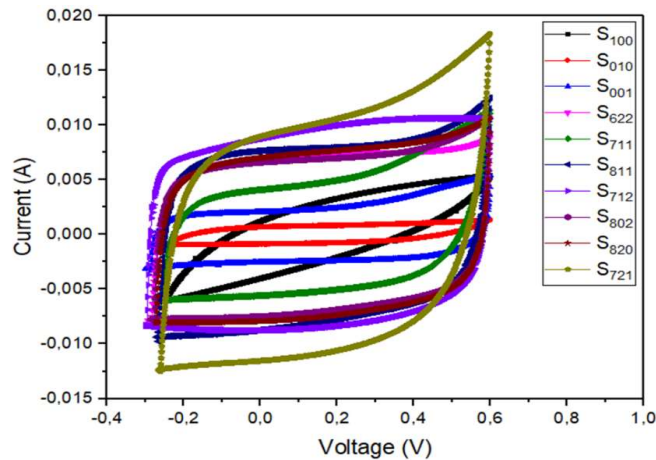


Figure 4 CV curves of the different samples at scan rates 2 mV s^{-1} in 6.0 M KOH aqueous electrolytes.

The material was combined and optimized to increase the capacitance of the supercapacitor. Optimization was carried out with a mix of designs that determine the effect of material interaction on capacitance. Each electrode sample was prepared by a mixture of materials to obtain 0.2 g . Table 1 shows the samples with a combination of materials and the results of electrochemical characterization of the supercapacitor. Table 1 shows that sample S_{721} , whose material consists of AC, MWCNT, and GR with 70, 20, and 10%, respectively, has the highest capacitance. The interactions occur between the components in the electrode and the capacitance or supercapacitor of a specific trend. The increased capacitance value indicates the combination of the large surface area possessed by activated carbon. The high conductivity of MWCNT and GR and the large pore size of MWCNT and GR increase the diffusion of electrolyte ions with a rise in the conductivity of the electrode material supercapacitor capacitance.

Optimization of Electrode Material Composition from Activated Carbon, MWCNT & Graphene to Enhance Performance of Supercapacitor

Table 1 Experimental design for the preparation of electrode material composition.

Sample	AC. (%wt)	MWCNT (% wt)	GR. (%wt)	Specific capacitance at 2 mV s ⁻¹ (F g ⁻¹)
S ₁₀₀	100	0	0	13.12
S ₀₁₀	0	100	0	3.93
S ₀₀₁	0	0	100	7.86
S ₈₀₂	80	0	20	21.30
S ₆₂₂	60	20	20	15.62
S ₈₂₀	80	20	0	24.71
S ₈₁₁	80	10	10	18.41
S ₇₁₂	70	10	20	21.29
S ₇₁₁	70	15	15	18.20
S ₇₂₁	70	20	10	33.12

The cyclic voltammograms (CV) of the different samples of EDLCs at a scan rate of 2 mV s⁻¹ in a 6 M KOH aqueous solution are shown in Figure 4. Aside from the S₇₂₁ piece, all other examples were similar to the rectangular shape and exhibited good symmetry, indicating ideal capacitive behavior. The CVs of SC using the S₇₂₁ sample in 6 M KOH were measured at various scan rates (see Figure 6a). The CV shapes of all coin-cell SCs in 6 M KOH exhibited slanted parallelogram loops, indicating high-power capabilities with a quick charge/discharge process, typical electrical double layer capacitor (EDLC) behavior, and low equivalent series resistance. Furthermore, it illustrated an additional current due to the faradaic mechanism. The current response increases with the rise in scan rate, indicating a reduction in electrode internal diffusion resistance [29].

The operating voltage of -0.3 to 0.6 V at different current densities was used to determine the Galvanostatic charge/discharge (GCD) measurements (see Figure 5(b)). Furthermore, the areas under CV curves were used to determine the capacitances with the values plotted as a function of scan rate for both negative and positive electrodes, as indicated in Figure 5(d).

EIS curves (Figure 5(c)) show the semicircular zone for the AC/MWCNT/GR composite is less than the pure AC, MWCNT, and GR. Therefore, the additions of MWCNT/GR decreased the interlayer resistance of the activated carbon sheets and the contact resistance with the current collector. The surrounding MWCNT can enhance the electronic conductivity of the AC and GR. Similarly, the AC particle tends to effectively suppress the re-stacking of the GR sheet and the aggregation of the MWCNT. Figure 5(c) shows a Nyquist plot with a 45° straight line from the lower left to the upper right; the Warburg curves indicate that the electrode material has enhanced access to the electrolytic ions [30-31].

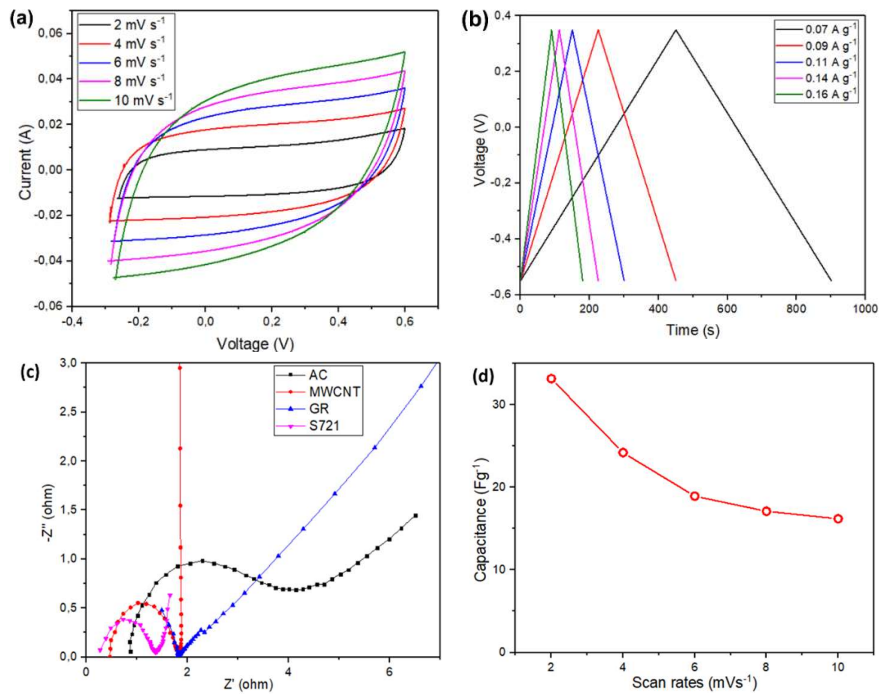


Figure 5 (a) CV curves of different scan rates in 6 M KOH aqueous electrolyte, (b) GCD curves of the sample at various current densities, (c) EIS curve for different electrode materials, and (d) the specific capacitance of the S₇₂₁ sample at different scan rates.

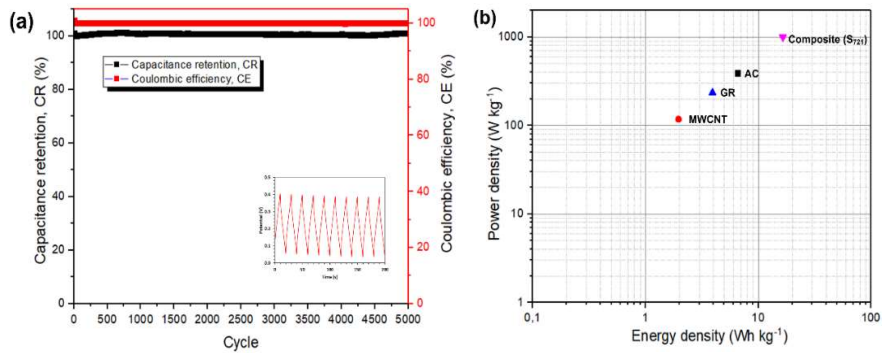


Figure 6 (a) Cyclic stability of composite (S₇₂₁) based-supercapacitor and (b) Ragone plot for pristine and composite based-supercapacitor.

Optimization of Electrode Material Composition from Activated Carbon, MWCNT & Graphene to Enhance Performance of Supercapacitor

The coulombic efficiency (CE) and capacitance retention (CR) determine the supercapacitor cycle stability. CE is the discharge capacity to charge capacity ratio in a given cycle. At the same time, CR is the ratio of each process capacitance to its initial capacitance [32-33]. Figure 6(a) shows that the CE and CR values for a composite electrode-based supercapacitor remained close to 100% for 5000 cycles. Figure 6(a) indicates that the composite material showed outstanding capacitance performance while maintaining constant voltage and operating current cell cycle stability. A high CE also means little risk of side reactions at the electrode surface [24, 34]. The energy and power density of the symmetric supercapacitor were displayed in the Ragone plot in Figure 6(b). Composite based-supercapacitor has the highest energy and power density compared to other cells, showing that composite materials improve supercapacitor performance.

3.3 Optimization of Electrode Material Composition

Minitab 19.1 is used to analyze and model an equation representing the trend of the experimental data shown in Table 1 with the equation shown in Eq. (2).

$$\begin{aligned} \text{Capacitance} = & 2.003AC + 41.24 \text{ MWCNT} + 32.97GR - 0.6002 AC \\ & \cdot \text{MWCNT} - 0.4990 AC \cdot GR - 2.560 \text{ MWCNT} \cdot GR \\ & + 0.03143 AC \cdot \text{MWCNT} \cdot GR \end{aligned} \quad (2)$$

These equations indicate that AC, MWCNT, and GR significantly contribute to the positive effect of the supercapacitor performance [35]. Besides, the interaction between these variables positively affects the electrode in the capacitance. Meanwhile, the interaction between AC and MWCNT, AC and GR, and MWCNT and GR in the electrode negatively affects the capacitance. Therefore, based on Eq. (2), surface and contour plots are obtained using Minitab, with the results shown in Figure 7.

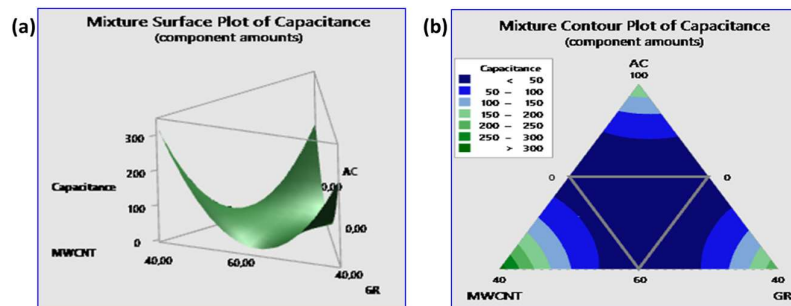


Figure 7 (a) Mixture surface plot of capacitance, (b) contour plot of capacitance.

The surface and contour plots shown in Figure 7 inform that the interaction between components is a factor capable of increasing the supercapacitor performance. This is shown in the resulting area in the plots, which are proportional to all materials. The composition of the material, which gives the optimal capacitance value, is shown in Figure 8. Therefore, based on the optimization curve, it is concluded that the combination of AC, MWCNT, and GR materials obtain optimum capacitance of 71.7%, 20%, and 8.3 wt%, respectively.

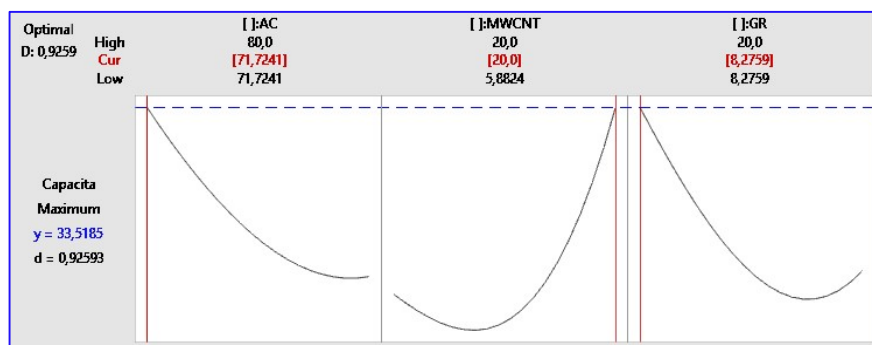


Figure 8 Optimization curve.

4 Conclusion

In conclusion, the electrode material from a composite mixture of AC, MWCNT, and GR can reduce ohmic and charge transfer resistance, thereby increasing capacitance significantly. Furthermore, the MWCNT that surrounds the AC and GR improves their electric conductivity. Similarly, the AC particle tends to effectively suppress the re-stacking of the GR sheet and the aggregation of the MWCNT. The optimum mixture composition of AC, MWCNT, and GR were 71.7%, 20%, and 8.3%wt, respectively, thereby producing the highest capacitance value of 33.5 F g^{-1} in 6 M KOH electrolyte. The advantages of optimized composite electrodes are obtained by comparing the results to EDLCs following the pure AC, MWCNT, and GR.

Acknowledgment

The author gratitude to the Palm Oil Fund Management Agency of the Indonesian Ministry of Finance for supporting this work during the fiscal year 2020/2021.

Optimization of Electrode Material Composition from Activated Carbon, MWCNT & Graphene to Enhance Performance of Supercapacitor

References

- [1] Zhao, Y., Lu, M., Tao, P., Zhang, Y., Gong, X., Yang, Z., Zhang, G.Q. & Li, H., *Hierarchically Porous and Heteroatom Doped Carbon Derived from Tobacco Rods for Supercapacitors*, Journal of Power Sources, **307**, pp. 391-400, 2016.
- [2] Wang, T., Shao, J., Wang, D. & Yang, Y.W., *Mesoporous Transition Metal Oxides for Supercapacitors*, Nanomaterials, **5**, pp. 1667-1689, 2015.
- [3] Simon, P. & Gogotsi, Y., *Perspectives for Electrochemical Capacitors and Related Devices*, Nature Materials, **19**, pp.1151-1163, 2020.
- [4] Fields, R., Lei, C., Markoulidis, F. & Lekakou, C., *The Composite Supercapacitor*, Energy Technology, **4**, pp. 517–525, 2016.
- [5] Park, S., Vosguerichian, M. & Bao, Z., *A Review of Fabrication and Applications of Carbon Nanotube Film-based Flexible Electronics*, Nanoscale, **5**, pp. 1727-1752, 2013.
- [6] Khalid, M., Bhardwaj, P. & Varela, H., *Carbon-Based Composites for Supercapacitor*, Sato, T (Ed.), Science, Technology and Advanced Application of Supercapacitors, London: IntechOpen, 2018.
- [7] Shirshova, N., Qian, H., Houllé, M., Steinke, J.H., Kucernak, A.R., Fontana, Q.P., Greenhalgh, E.S., Bismarck, A. & Shaffer, M.S., *Multifunctional Structural Energy Storage Composite Supercapacitors*, Faraday Discussions, **172**, pp. 81-103, 2014.
- [8] Candelaria, S.L., Garcia, B.B., Liu, D. & Cao, G.Z., *Nitrogen Modification of Highly Porous Carbon for Improved Supercapacitor Performance*, Journal of Materials Chemistry, **22**, 9884, 2012.
- [9] Simon, P. & Gogotsi, Y., *Capacitive Energy Storage in Nanostructured Carbon Electrolyte Systems*, Accounts of Chemical Research, **46**, pp. 1094-1103, 2013.
- [10] Hao, L., Li, X. & Zhi, L., *Carbonaceous Electrode Materials for Supercapacitors*, Advance Material, **25**, pp. 3899-3904, 2013.
- [11] El-Kady, M.F., Shao, Y. & Kaner, R.B., *Graphene for Batteries, Supercapacitors and Beyond*, Nature Review Material, **1**, pp.1–14. 2016.
- [12] Chen, Y., Zhang, X., Zhang, H., Sun, X., Zhang, D. & Ma, Y., *High-Performance Supercapacitors Based on a Graphene-Activated Carbon Composite Prepared by Chemical Activation*, RSC Advance, **2**, pp. 7747-7753, 2012.
- [13] Raza, W., Alib, F., Razac, N., Luoa, Y., Kim, K.H., Yanga, J., Kumar, S., Mehmooda, A. & Kwon, E.E., *Recent Advancements in Supercapacitor Technology*, Nano Energy, **52**, pp.441-473, 2018.
- [14] Sianipar, M., Kim, S.H. & Iskandar, F., *Functionalized Carbon Nanotube (CNT) Membrane: Progress and Challenges*. RSC Advance, **7**, pp. 51175-51198, 2017.

- [15] Zheng, C., Zhou, X.F., Cao, H.L., Wang, G.H. & Liu, Z.P., *Synthesis of Porous Graphene/ Activated Carbon Composite with High Packing Density and Large Specific Surface Area for Supercapacitor Electrode Material*, Journal of Power Sources, **258**, pp. 290-296, 2014.
- [16] Trogadas, P., Fuller, T.F. & Strasser, P., *Carbon as Catalyst and Support for Electrochemical Energy Conversion*, Carbon, **75**, pp.5-42, 2014.
- [17] Gudavalli, G. & Dhakal, T., *A Materials Review in Emerging Materials for Energy Conversion and Storage (Newyork: Elsevier)*, 274, 2018.
- [18] Wang, Y., Wu, Y., Huang Y., Zhang, F., Xi Y., Ma, Y. & Chen., Y., *Preventing Graphene Sheets from Restacking for High-Capacitance Performance*, The Journal of Physical Chemistry C, **115**, pp. 23192-23197, 2011.
- [19] Yu, A., Chabot, V. & Zhang, J., *Electrochemical Supercapacitors for Energy Storage and Delivery. Fund. Apply (Boca Raton: CRC Press)*, 373, 2013.
- [20] Cheng, F., Yang, X., Zhang, S. & Lu, W., *Boosting The Supercapacitor Performances of Activated Carbon with Carbon Nanomaterials*, Journal of Power Sources, **450**, 227678, 2020.
- [21] Xu, C., Xu, F., Sun, L., Cao, F., Yu, F., Zhang, H., Yan, E., Peng, H., Chu, H. & Zou. Y., *A High-Performance Supercapacitor Based On Nitrogen-Doped Porous Carbon Derived from Cycas Leaves*, International Journal of Electrochemical Science, **14**, pp.1782-1793, 2019.
- [22] Clemente, J. S., Beauchemin, S., Thibault, Y., Ted MacKinnon, & Smith, D., *Differentiating Inorganics in Biochars Produced at Commercial Scale Using Principal Component Analysis*, ACS Omega, **3**, pp. 6931-6944; 2018.
- [23] Adinaveen, T., Vijaya, JJ, L. & Kennedy. LJ, *Comparative Study of Electrical Conductivity On Activated Carbons Prepared from Various Cellulose Materials*, Arab J Sci Eng. **41**, pp. 55-65. 2016.
- [24] M. Barczak, & Bandosz, T.J., *Evaluation of Nitrogen- And Sulfur-Doped Porous Carbon Textiles as Electrode Materials for Flexible Supercapacitors*, Electrochim. Acta, **305**, pp. 125-136, 2019.
- [25] Ivanov, E., Kotsilkova, R., Xia, H., Chen, Y., Donato, R.K., Donato, K., Godoy, AP, Di Maio, R., Silvestre, C., Cimmino, S. & Angelov, V., *PLA/Graphene/MWCNT Composites with Improved Electrical and Thermal Properties Suitable for Fdm 3d Printing Applications*, Applied Science, **9**, 1209, 2019.
- [26] Liu, J., Deng, Y., Li, X. & Wang, L., *Promising Nitrogen-Rich Porous Carbons Derived from One-Step Calcium Chloride Activation of Biomass-Based Waste for High-Performance Supercapacitors*, ACS Sustainable Chemical Engineering, **4**, pp.177-187, 2016.

Optimization of Electrode Material Composition from Activated Carbon, MWCNT & Graphene to Enhance Performance of Supercapacitor

- [27] Liang, K., Wang, W., Yu, Y., Liu, L., Haijun, L., Zhang, Y. & Chen, A., *Synthesis of Nitrogen-Doped Mesoporous Carbon for High-Performance Supercapacitors*, New Journal of Chemistry, **43**, pp. 2776-2782, 2019.
- [28] Markoulidis, F., Lei, C., Lekakou, C., Duff, D., Khalil, S., Martorana, B. & Cannavaro, I., *A Method to Increase the Energy Density Supercapacitor Cells by The Addition of Multiwall Carbon Nanotubes into Activated Carbon Electrodes*, Carbon, **68**, pp. 58-66, 2014.
- [29] Zheng, Z. & Gao, Q., *Hierarchical Porous Carbons Prepared by Easy One-Step Carbonization and Activation of Phenol-Formaldehyde Resins with High Performance for Supercapacitors*, Journal of Power Sources, **196**, pp.1615–1619, 2011.
- [30] Wang, L., Gao, Z., Chang, J., Liu, X., Wu, D., Xu, F., Guo, Y. & Jiang., K., *Nitrogen-Doped Porous Carbon as Electrode Materials for High-Performance Supercapacitor and Dye-Sensitized Solar Cell*, ACS Applied Material Interfaces, **7**(36), pp.20234-20244, 2015.
- [31] Li, X., Tang, Y., Song, J., Yang, W., Wang, M., Zhu, C., Zhao, W., Zheng, J. & Lin, Y., *Self-Supporting Activated Carbon/Carbon Nanotube/Reduced Graphene Oxide Flexible Electrode for High-Performance Supercapacitor*, Carbon, **129**, pp.236-244, 2018.
- [32] Zhang, F., Zhang, T., Yang, X., Zhang, L., Leng, K., Huang, Y. & Chen, Y., *High-Performance Supercapacitor-Battery Hybrid Energy Storage Device Based on Graphene-Enhanced Electrode Materials with Ultrahigh Energy Density*, Energy Environmental Science, **6**, pp. 1623-1632., 2013.
- [33] Balducci A., Belanger, D., Brousse, T., Long, J.W. & W. Sugimoto, *A Guideline for Reporting Performance Metrics with Electrochemical Capacitors: From Electrode Materials to Full Devices*, Journal of The Electrochemical Society, **164**(7), pp. A1487-A1488, 2017.
- [34] Rustamaji, H., Prakoso, T., Devianto, H., Widiatmoko, P. & Saputera, W. H., *Urea Nitrogenated Mesoporous Activated Carbon Derived from Oil Palm Empty Fruit Bunch for High-Performance Supercapacitor*, Journal of Energy Storage, **52**, 104724, 2022.
- [35] Markoulidis F., Todorova, N., Grilli, R., Lekakou, C. & Christos Trapalis, C., *Composite Electrodes of Activated Carbon and Multiwall Carbon Nanotubes Decorated with Silver Nanoparticles for High Power Energy Storage*, Journal of Composites Science, **3**(97), pp.2-13, 2019.